Noname manuscript No.
(will be inserted by the editor)

Simulating dispersion in the evening-transition boundary layer

Alexander C. Taylor · Robert J. Beare · David J. Thomson

Received: date / Accepted: date

Abstract We investigate dispersion in the evening-transition boundary layer using large-eddy simulation (LES). In the LES, a particle model traces pollutant paths using a combination of the resolved flow velocities and a random displacement model to represent subgrid-scale motions. The LES is forced with both a sudden switch-off of the surface heat flux and also a more gradual observed evolution. The LES shows 'lofting' of plumes from near-surface releases in the pre-transition convective boundary layer; it also shows the subsequent 'trapping' of releases in the post-transition near-surface stable boundary layer and residual layer above. Given the paucity of observations for pollution dispersion in evening transitions, the LES proves a useful reference.

We then use the LES to test and improve a one-dimensional Lagrangian Stochastic Model (LSM) such as is often used in practical dispersion studies. The LSM used here includes both time-varying and skewed turbulence statistics. It is forced with the vertical velocity variance, skewness and dissipation from the LES for particle releases at various heights and times in the evening transition. The LSM plume spreads are significantly larger than those from the LES in the post-transition stable boundary-layer trapping regime. The forcing from the LES was thus insufficient to constrain the plume evolution, and inclusion of the significant stratification effects was required. In the so-called modified LSM, a correction to the vertical velocity variance was included to represent the effect of stable stratification and the consequent presence of wave-like motions. The modified LSM shows improved trapping of particles in the post-transition stable boundary layer.

Keywords Dispersion · Evening transition · Lagrangian stochastic model · Large-eddy simulation

1 Introduction

The atmospheric boundary layer (ABL) over land typically experiences a strong diurnal cycle forced by solar radiation. Surface heating drives convective boundary-layer (CBL) turbulence in the daytime, and surface cooling leads to a stable boundary layer (SBL) at night. In the

Dr A. C. Taylor and Dr R. J. Beare (corresponding author)
College of Engineering, Mathematics and Physical Sciences, University of Exeter, UK. EX4 4QF. Email: r.j.beare@ex.ac.uk

Dr D. J. Thomson
Met Office, Exeter, UK.

evening, the sensible heat flux diminishes in response to the sun's decreasing elevation, resulting in the dissipation exceeding the production of turbulent kinetic energy (TKE), and in the decay of large-scale convective eddies. The evening and morning transitions feature a period of rapid evolution in the state of the turbulence compared with other times in the diurnal cycle.

Dispersion models have a range of important applications, including: producing air-quality forecasts, planning the placement of industry, deciding on the requirements for chimney-stack heights, and tracking the paths of dangerous pollutants and issuing warnings in events such as the Fukushima Daiichi nuclear accident, or the eruption of the Icelandic volcano Eyjafjallajökull. For such models to be effective they must predict the path of the pollution accurately. However, the effect of rapidly time-varying turbulence (such as in the boundary-layer evening transition) is often highly idealized or overlooked. In this paper we use a large-eddy simulation (LES) and a Lagrangian stochastic model (LSM) to study this problem.

1.1 Large-Eddy Simulation

LES models fluid flow in situations where the Reynolds number is large. Turbulent eddies larger than the grid scale are solved explicitly using the momentum, thermodynamic and continuity equations, while smaller scale motions are represented by a subgrid model. LES provides a 3D representation of the flow and includes many of the processes at work in the atmosphere, and hence provides the best substitute for experimental data, with the advantage of being adaptable to the conditions one wishes to simulate.

A dispersion model may be included in the LES by specifying initial particle positions, and advancing them by applying the local flow velocity at each timestep, along with a random perturbation to account for subgrid-scale motions. This method has previously been used to describe dispersion in the CBL by Mason (1992) and Weil et al. (2004), and in the SBL by Kemp and Thomson (1996).

1.2 Lagrangian Stochastic Model

LSMs are often used to simulate turbulent dispersion in the atmospheric boundary layer. The use of such models began with the work of Taylor (1921) who considered transport by homogeneous turbulence, and has continued with key advances such as:

- Modelling dispersion in inhomogeneous turbulence in the atmospheric surface layer with comparisons to experimental data, for example, by Wilson et al. (1981).
- Work by Thomson (1984), van Dop et al. (1985), Sawford (1986), Thomson (1987) and others on the conditions that should be satisfied in LSMs for turbulent diffusion. In particular, they established the well-mixed criterion, which states that, "If the particles of a tracer are initially well-mixed (in position-velocity space) in a turbulent flow, they should remain so."

LSMs have also been applied to incorporate and describe the effects of important features of atmospheric boundary-layer turbulence on dispersion, such as the asymmetry of top-down and bottom-up diffusion (Weil, 1990). A short review of the use of LSMs to describe turbulent diffusion may be found in Chapter 2 of Rodean (1997) or in Wilson and Sawford (1996).

1.3 Evening-transition boundary layer

The ABL is typically categorized into three states governed by surface heating: stable, neutral and convective. Boundary-layer transitions occur when the surface heating is added or removed, which generally occurs at sunrise and sunset. This process has been modelled by Nieuwstadt and Brost (1986), Sorbjan (1997), Goulart et al. (2003), Pino et al. (2006) and Beare et al. (2006), among others. During boundary-layer transitions the turbulence properties are strongly time dependent, and the problem of dispersion in such time-dependent flows has not been addressed much in the literature. Here, we address this gap in the literature by performing both LES and LSM simulations of dispersion for the evening transition. Given the paucity of observations of pollution dispersion in the evening transition, the LES is used as a reference against which the strengths and weaknesses of the LSM can be identified.

To date, there has been limited research into modelling dispersion during the boundary-layer evening transition. Carvalho et al. (2010) studied dispersion in decaying turbulence using a LSM where the turbulence was represented by time-varying eddy diffusivities. Although an approximation, this study provides a useful insight into the role of the residual layer and the SBL in determining pollution concentrations. However, the LSM is only compared with itself. There is thus significant scope for further investigation using LES as a reference: the first aim is to determine the impact of the evening transition on dispersion using LES. The LSM is then compared with the LES in order to identify improvements in its formulation.

2 Method

2.1 LES

The Met Office large-eddy model (Gray et al., 2004) is employed to simulate boundary layers over the duration of an evening transition using periodic lateral boundary conditions. Two cases of the evening transition are simulated using idealized and observed forcings respectively; we describe these cases below.

2.1.1 Idealized forcing

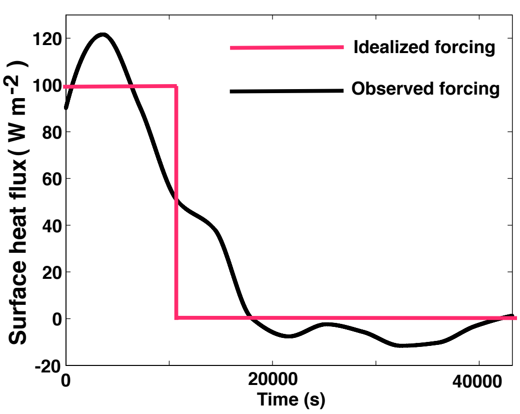

Fig. 1: Surface sensible heat flux plotted against time from the start of the simulation for the idealized forcing (red) of Nieuwstadt and Brost (1986) and the observed forcing (black) from the Cardington site for the evening of 23 September 2003.

The first case is the idealized decay of a CBL described by Nieuwstadt and Brost (1986). Here the positive surface sensible heat flux is suddenly changed to zero. The Nieuwstadt and Brost (1986) case will allow us to focus on the role of the decaying residual layer in dispersion. The residual layer herein refers to the weakly stratified region with a depth similar to the preceding CBL. This contrasts with the post-transition SBL that occurs for the observed forcing (see Sect. 2.1.2) which has a depth significantly smaller than the preceding CBL and is more strongly stratified. The geostrophic wind vector is directed along the x-direction and is of magnitude 5 m s^{-1}. The roughness length is set at 0.01 m for momentum and heat. The initial potential temperature is a constant 283 K from the surface to 800 m, with a capping inversion of 0.0025 K m^{-1} from 800 m to the domain top. Figure 1 shows the time evolution of the surface sensible heat flux for the idealized forcing. A constant surface heating of 100 W m^{-2} is applied to generate convective turbulence. The model is initially run for 10,800 s, by which time the turbulence has become statistically stationary. At this time the surface sensible heat flux is set instantaneously to zero to simulate the decay of convective turbulence. For the idealized forcing, a shallow SBL does not form as the surface sensible heat flux does not go negative. Eventually the decay will stop and form a neutral boundary layer with stratification above. The stratification effects will thus be entirely due to the residual layer. A reference time coordinate (t_d) is introduced such that $t_d = 0$ at the start of the transition (t = 10,800 s). A domain size of $5 \times 5 \times 4$ km^3 is used (the last number is the vertical extent), with 100×100 grid points in the horizontal, and 90 points of variable resolution in the vertical. The horizontal grid length is 50 m and the vertical grid is refined near the surface and stretched above the CBL.

2.1.2 Observed forcing

In order to consider the role of the post-transition SBL, the second case uses the observed forcing of Beare et al. (2006). The time evolution of the surface sensible heat flux is shown in Fig. 1. Unlike the idealized forcing, there is now a negative nighttime sensible heat flux after the transition leading to the development of a SBL. Such a developing SBL is more stratified than the overlying residual layer, and strongly inhibits the vertical transport of pollution leading to high concentrations in the SBL (trapping). In order to resolve the SBL, the LES is run with a 10-m horizontal resolution and variable vertical resolution (with a 10-m vertical grid length in the SBL) over $256 \times 256 \times 90$ grid points and on a domain of $2.56 \times 2.56 \times 2$ km^3. The model is initialized with a uniform potential temperature up to 800 m with an overlying inversion of strength 0.0025 K m^{-1}. The geostrophic wind vector is directed along the x-direction and is of magnitude 7 m s^{-1}.

2.1.3 Trajectory calculation

Particle trajectories in the LES are calculated using a combination of the resolved flow velocity and a representation of the subgrid-scale motions at each timestep, following Kemp and Thomson (1996). The vector displacement of the particle ($\Delta\mathbf{x}$) is calculated with an Euler forward step method using the current LES timestep (Δt), the LES resolved velocity ($\mathbf{u}$) interpolated to the particle position, random vector displacements ($\mathbf{R}_d$) and a drift correction velocity (∇K) where K is the LES eddy diffusivity interpolated to the particle position,

$$\Delta\mathbf{x} = \mathbf{u}\Delta t + \mathbf{R}_d + \nabla K \Delta t. \tag{1}$$

The random perturbations follow a Gaussian distribution with standard deviation given by

$$\sigma_d = (2K\Delta \mathrm{t})^{1/2}. \tag{2}$$

Gaussian random numbers are generated numerically using the Box-Müller transform (Box and Müller, 1958). The prescription of this random perturbation generates a mean drift towards regions of small K and this is corrected by adding the drift correction velocity. In areas of the flow where the size of the eddies is smaller than the grid length, the resolved TKE tends to zero. In these regions, such as near the surface, the representation of the subgrid energy via the random vector displacements becomes essential. Periodic lateral boundary conditions are applied to the particle model, as in the LES.

2.2 LSM

We first describe the standard form of the LSM for vertical dispersion in stationary, horizontally-homogeneous flows with Gaussian velocity distributions and then the modified form that we are using for transitional boundary layers. The equations describing the evolution of particle vertical velocity w and vertical position z are

$$dw = a(z, w)dt + b(z, w)d\xi, \tag{3}$$

$$dz = wdt, \tag{4}$$

where $d\xi$ is a Gaussian random forcing with zero mean and variance dt and a and b are functions. In the standard LSM, the functions a and b are given by

$$a = -\frac{C_0 \epsilon w}{2\sigma_w^2} + \frac{1}{2}\left(1 + \frac{w^2}{\sigma_w^2}\right)\frac{\partial \sigma_w^2}{\partial z}, \tag{5}$$

$$b = (C_0 \epsilon)^{1/2}, \tag{6}$$

where C_0, σ_w^2 and ϵ are a dispersion parameter (formally equal to the inertial subrange constant in the Lagrangian velocity structure function, but often regarded as a tunable parameter to describe the dispersion), the vertical velocity variance and the rate of dissipation of TKE per unit mass respectively. The first term in Eq. 5 is deterministic and represents the fading memory of the particle velocity from earlier times; the second term in Eq. 5 is the deterministic drift correction term. The vertical gradient of σ_w^2 forces particles away from regions of small σ_w^2 ensuring they become well-mixed in the domain over time and preventing their accumulation in regions of small σ_w^2 that would otherwise occur. The function in Eq. 6 sets the amplitude of the random process. For further details of vertical dispersion in stationary flows with Gaussian velocity distributions see e.g. Rodean (1997).

In this study, we modify the standard LSM by allowing skewed velocity distributions following Luhar and Britter (1989) and by introducing a time dependence to the functions a and b, thus allowing the consideration of non-stationary, skewed turbulence such as occurs at the start of the evening transition. The resulting function a is an extension of the form proposed by Hudson and Thomson (1994). The derivation is complex so the details are summarized in the Appendix. Herein, we refer to this model as 'the LSM'. We use a value of $C_0 = 2$ following Luhar and Britter (1989), and, as is common in other LSMs, a reflection boundary condition is applied at the CBL top.

Within the LSM the state of turbulence is defined by vertical profiles of the vertical velocity variance, the dissipation of TKE, and the skewness of vertical velocities ($\overline{w^3}$). Normally these profiles have been represented in two ways. The first is as functions continuous in the range $0 \leq z \leq h$ (where h is the height of the ABL) with amplitudes dependent on the friction velocity

(u_*), the convective velocity scale (w_*) and the length scales h and the Obukhov length (L). These functions are derived by finding a best fit to observed profiles; the method is detailed in Chapter 12 of Rodean (1997). The second approach, and the one adopted here, is to utilize a more complex model such as LES to determine the turbulence profiles, and then use these directly in the LSM, as done previously by Weil et al. (2004). Driving the LSM with LES turbulence profiles and comparing dispersion concentrations between both models provides a test of whether the formulation of the LSM and the boundary-layer specification in the LSM are sufficient. If there is disagreement in the dispersion concentrations, then more detailed boundary-layer properties may be required.

2.3 Modified LSM

The decay of turbulence caused by the instantaneous switch-off of surface heat flux leads to the development of a positive potential temperature gradient over the depth of the residual layer. Such a stably stratified layer may support both gravity waves and turbulence, with large-scale vertical motions suppressed by the stability (Stull, 1988). The LSM has been previously modified by Das and Durbin (2005) for stratified flows. Their method involved matching the LSM to the corresponding second-order closure equations for stratified flows. We adopt a simpler approach in terms of defining the key length scales and modifying the vertical velocity variance in the LSM, with the aim of removing the contribution from waves. The natural length scale defining the separation between gravity waves and turbulence is the Ozmidov scale (L_o),

$$L_o = \epsilon^{\frac{1}{2}} N^{-\frac{3}{2}}, \tag{7}$$

where N is the Brunt-Väisälä frequency. For length scales larger than L_o gravity waves tend to dominate, whilst for smaller scales turbulence prevails. We argue that gravity waves disperse much less efficiently than turbulence in the stratified boundary layer, and thus we need to modify the vertical velocity variance forcing the LSM to account for this effect. We represent dissipation as

$$\epsilon = D\frac{\sigma_w^3}{l}, \tag{8}$$

where D is a constant and σ_w^2 and l are the variance and length scale of the turbulent part of the fluctuations. If we set $l = L_o$ we find that the maximum value for the turbulent variance is of order

$$\sigma_w^2 = E\frac{\epsilon}{N}, \tag{9}$$

where E is a constant. Equation 9 thus defines the threshold between waves and turbulence. For $\sigma_w^2 > E\epsilon/N$ gravity waves predominate and turbulence dominates otherwise. Since the gravity waves are poor at dispersion, we define a modified, 'turbulence only', vertical velocity variance ($\sigma_{w_{mod}}^2$) as

$$\sigma_{w_{mod}}^2 = \min\left(\sigma_w^2, \frac{E\epsilon}{N}\right). \tag{10}$$

We refer to the LSM using the modified vertical velocity variance ($\sigma_{w_{mod}}^2$) as 'the modified LSM'. A value of $E = 1$ is used. The modified vertical velocity variance also conveniently takes the place of the reflection boundary condition used at the CBL top in the LSM; it naturally reduces spread above the CBL top.

2.4 Plume statistics

Plume behaviour is evaluated through statistical properties of a large ensemble of simulated particle trajectories. The plume centreline and spread are determined by finding the mean ($\overline{z_p}$) and standard deviation (σ_z) of the vertical position of all particles at any given timestep, using

$$\overline{z_p} = \left(\sum_{j=1}^{N_t} z_{p_j} \right) / N_t, \tag{11}$$

$$\sigma_z = \sqrt{\frac{1}{N_t} \sum_{j=1}^{N_t} \left(z_{p_j} - \overline{z_p} \right)^2}, \tag{12}$$

where the z_{p_j} are the particle heights, and N_t is the total number of particles being tracked.

In addition we consider vertical concentration profiles at various times. The vertical concentration profile is calculated by splitting the vertical axis into slices of depth Δz and counting the number of particles in each slice (N_z). The concentration at each level is then given by $N_z/\Delta z$. This may be normalized by the total number of particles, N_t, divided by the CBL height at the start of the transition, z_i, such that the concentration equals 1 when the particles are well-mixed. z_i is defined as the height of the sensible heat flux minimum. The normalized concentration at a given height (C_z) is thus given by

$$C_z = \frac{N_z z_i}{N_t \Delta z}. \tag{13}$$

3 Results

Prior to investigating the effect of the transition on particle trajectories, the evolution of the state of turbulence in the boundary layer is examined through vertical profiles of potential temperature, vertical heat flux, vertical velocity variance, dissipation rate of TKE, and the third moment of vertical velocity (Figs. 2a, 2b, 3a, 3b, and 3c respectively) for the idealized forcing.

The decay of turbulence caused by the instantaneous switch-off of surface heat flux leads to the development of a slightly positive potential temperature gradient with height over the extent of the residual mixed layer (Fig. 2a). This effect has been shown to be a robust feature of the decaying CBL in the LESs of Nieuwstadt and Brost (1986) and Pino et al. (2006), and in the observations discussed in Grant (1997). This feature can be seen to develop rapidly (within 400 s of the start of the switch-off of surface heat flux) and strengthen over the course of the transition (shown by the profile at t_d = 800 s). The positive potential temperature gradient suppresses vertical motions, which is expected to have an effect on particle dispersion. This is investigated below.

The normalized profile of sensible heat flux (Fig. 2b) shows how the development of a positive potential temperature gradient occurs. Before the transition, a negative gradient of sensible heat flux over the majority of the boundary layer indicates that transport of heat from the surface is warming the boundary layer. Shortly after the start of the transition (t_d = 400 s), the sensible heat flux near the surface has a positive gradient indicating cooling, while the upper part of the boundary layer continues to warm. Nieuwstadt and Brost (1986) refer to this process as ‘demixing’.

In Fig. 3, the solid lines represent daytime convective turbulence conditions at $t_d = 0$. Once the surface sensible heating is removed, all three profiles decay rapidly. By t_d = 1200 s, the peak vertical velocity variance has approximately halved, as shown in Fig. 3a. Also the peak has

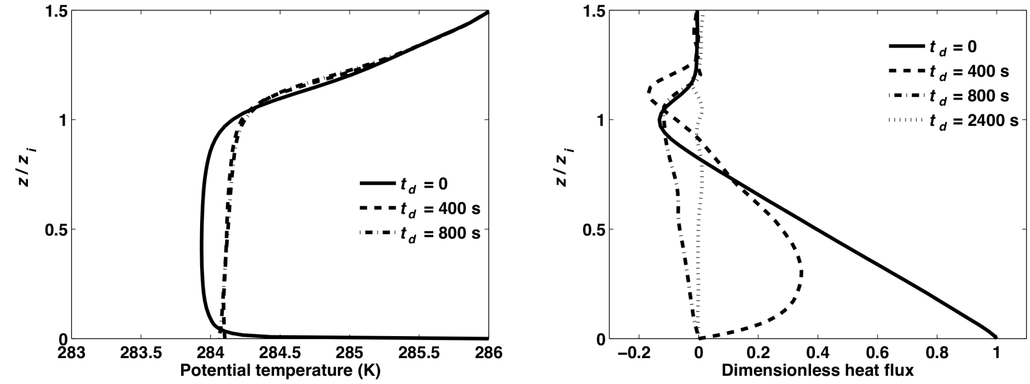

(a) (b)

Fig. 2: Profiles of (a) potential temperature and (b) sensible heat flux (normalized by the pre-transition surface sensible heat flux) plotted against height (normalized by inversion depth) at various times for the idealized forcing case (see legends).

moved upwards, close to the mid-height of the boundary layer indicating a more symmetrical eddy structure as observed by Nieuwstadt and Brost (1986). At later times, the vertical velocity variance at the mid-point of the boundary layer continues to decay, while shear-driven turbulence maintains velocity variance near the surface. Above the original CBL top, the variance does not decay as it does over the rest of the layer. This shows that the free atmosphere is not rapidly responding to the changes in surface forcing in the same way as the boundary layer, and suggests that this velocity variance may be attributed to non-turbulent motions. The third moment of vertical velocity rapidly decays to approximately zero throughout the boundary layer (Fig. 3c), and the dissipation is sustained near the ground as a result of shear-driven turbulence (Fig. 3b).

3.1 Particle Dispersion in LES

To investigate the mean dispersive effect of the boundary-layer turbulence, particles are released in a uniform square grid spanning the horizontal domain of the model at a given height. The trajectories are calculated using the LES with the idealized forcing, with releases at times $t_d = 0$ and $t_d = 1200$ s, three release heights spanning the depth of the pre-transition CBL and 90,000 particles per release.

Figure 4a shows the mean plume height for particles released from three different levels at $t_d = 0$. The plumes released from low and mid levels tend to a mean height of approximately $z_i/2$ after 3000 s ($z_i = 1374$ m). The particles have thus become well-mixed throughout the layer, and so their horizontally integrated concentration will be unaffected by further decay of the CBL. The plumes released near the boundary-layer top deviate less from their starting point. This is due to the decay of TKE near the boundary-layer top.

The plume structure is shown further by the standard deviation (σ_z) for the same three simulations (Fig. 4b). Particles from both the low-level and mid-level releases spread out rapidly, with σ_z reaching 400 m. With a sharp boundary-layer capping inversion we would expect a uniform concentration profile up to some specified height; in this context we note that $\sigma_z = 400$ m corresponds to a uniform distribution of depth 1386 m, using the theoretical result $\sigma_z =$

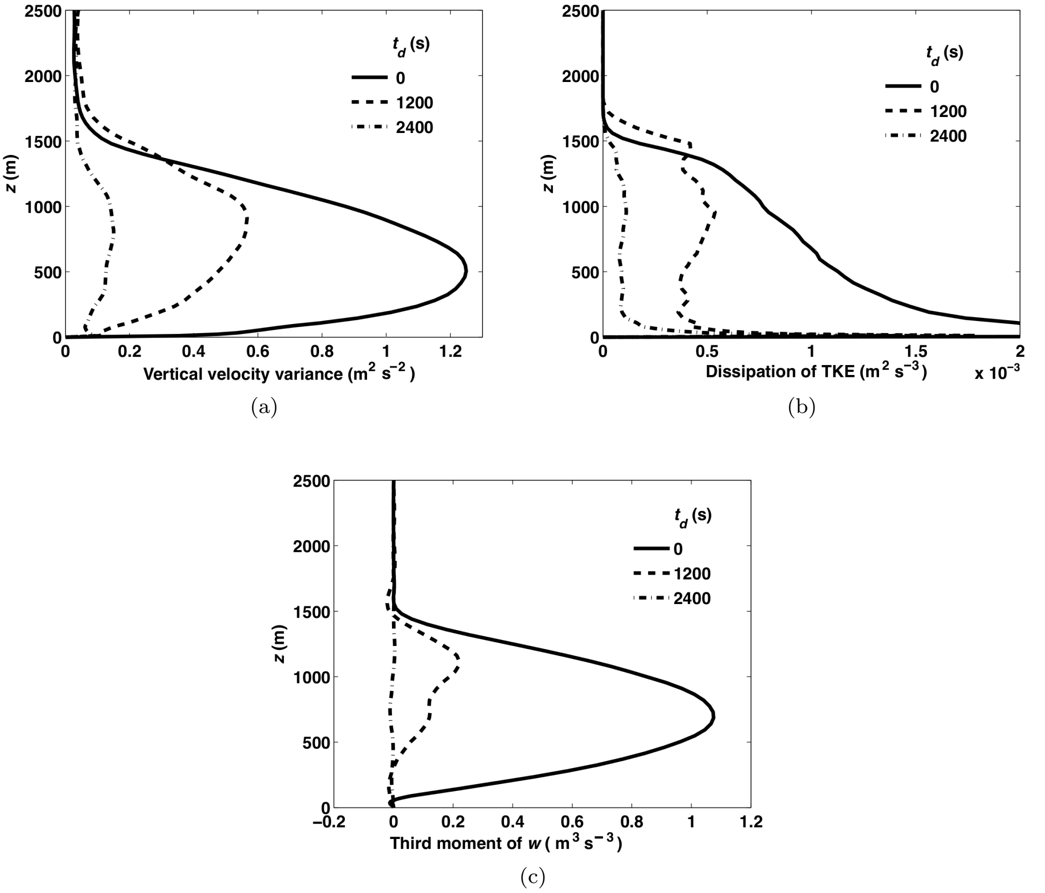

Fig. 3: Vertical profiles from the LES using the idealized forcing. Shown are (a) vertical velocity variance (resolved plus subgrid), (b) dissipation of TKE and (c) the third moment of vertical velocity at various times (t_d) after the switch-off of surface heat flux.

depth/$\sqrt{12}$, and this is close to the actual boundary-layer depth of 1374 m. In the high release case, however, the particles disperse less rapidly and tend to a smaller spread at large times. This also indicates a reduction of TKE near the boundary-layer top early in the transition.

Figure 4c shows the mean plume height for particles released from the same heights as in Fig. 4a but at $t_d = 1200$ s. In this case, the mean height deviates little from the release height over time. The reduced dispersion is also indicated by the standard deviation of these plumes, with slower initial rates of spread and with σ_z tending to a smaller value of only 200 m in the case of the high and low releases. The mid-level release has a larger standard deviation indicating more motion near the middle of the boundary layer. This is supported by the profile of vertical velocity variance in Fig. 3a. Before the transition, large-scale turbulent eddies, driven by surface heating, transport and mix material over the entire depth of the boundary layer. After the transition the large eddies decay, and mixing and vertical velocities are greatly reduced.

We now compare the LES particle simulations for a steady-state CBL with the experimental water-tank data of Willis and Deardorff (1976) and Willis and Deardorff (1978). Figure 5 shows

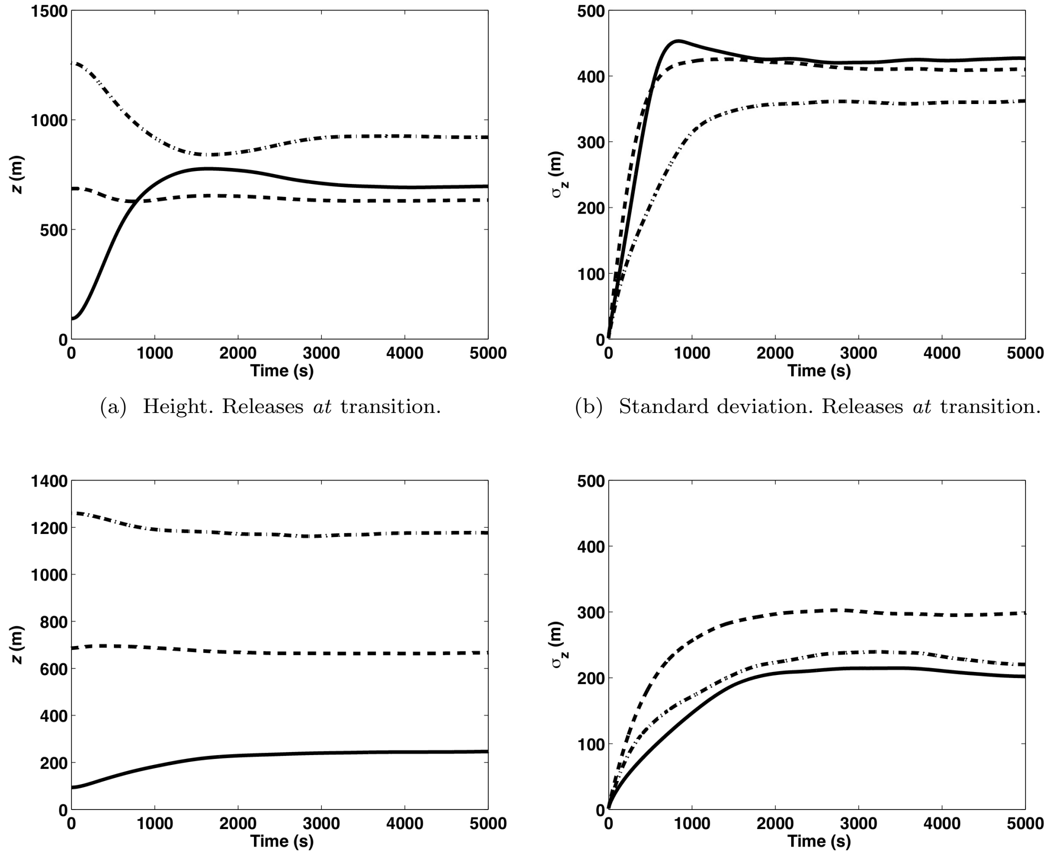

(a) Height. Releases *at* transition.

(b) Standard deviation. Releases *at* transition.

(c) Height. Releases *after* transition.

(d) Standard deviation. Releases *after* transition.

Fig. 4: Plume mean heights and standard deviations for releases from a range of heights at $t_d = 0$ ((a) and (b)) and at $t_d = 1200$ s ((c) and (d)) for the idealized forcing. Release heights are at 100 m (solid), 687 m (dashed) and 1260 m (dot-dashed). Inversion depth at $t_d = 0$ is 1374 m.

close agreement between the LES and the water-tank data. This validates our method for the CBL regime and gives us additional confidence in the dispersion results for the decaying-turbulence regime.

The trapping of particles close to their release height in the rapid transition leads to higher concentrations than occur when the particles are strongly mixed. This is demonstrated by Figs. 6a and 6b where the height distribution of particle concentrations for releases before and after the transition is given for a release height of 100 m. For the pre-transition release ($t_d = -1200$ s), particles mix over a deep layer and hence have a low concentration. However, for the post-transition release ($t_d = 1200$ s), particles do not disperse away from their release height so easily and remain in a shallow band at high concentrations. In order to understand this result further, it is instructive to consider the characteristic physical scales after the transition, namely the buoyancy scale z_b defined by $z_b = \sigma_w/N$. For this case $z_b \sim 150$ m and is the same order of magnitude as σ_z (Fig. 4d) indicating that particle dispersion is strongly influenced by the stratification.

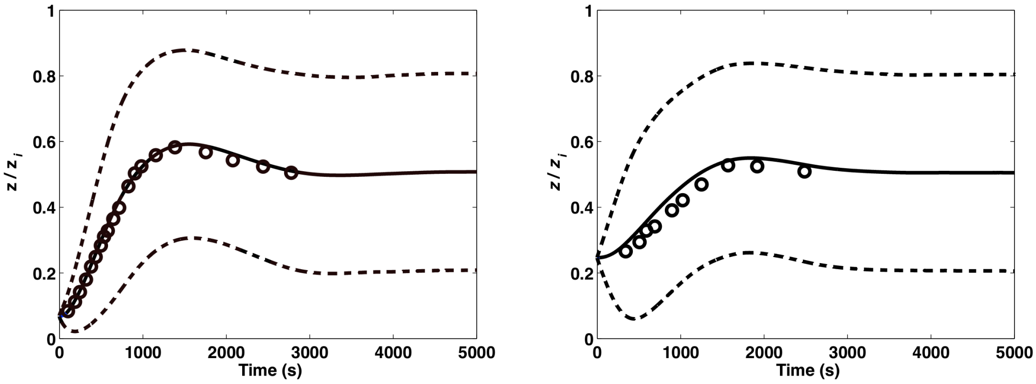

(a) (b)

Fig. 5: Plume height normalized by z_i plotted against time for a steady-state CBL. Results for the LES (solid) and one standard deviation either side (dashed) are shown for release heights of: (a) $z/z_i = 0.067$ and (b) $z/z_i = 0.24$. Plotted as circles are the experimental water-tank data of plume height from Willis and Deardorff (1976) and Willis and Deardorff (1978).

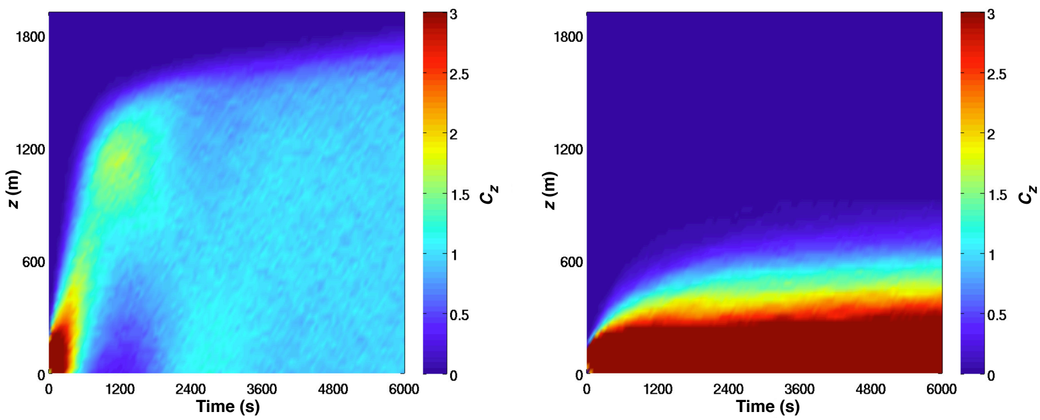

(a) Release before transition (b) Release after transition

Fig. 6: Particle concentration (C_z) from a near-surface release occurring at (a) $t_d = -1200$ s and (b) $t_d = 1200$ s where t_d is the time after the switch-off of surface heat flux. Particles are released at height $z = 100$ m for the idealized forcing. Note that the time of the release shown in frame (a) is earlier than the time $t_d = 0$ used in the other figures.

3.2 LSM and modified LSM predictions

Trajectories are also calculated using the LSM for release times of $t_d = 0$ and $t_d = 1200$ s and for release heights near the surface, at a mid-level and at a high-level. As in the LES, 90,000 particles are used per release. Figure 7 shows the mean plume heights and standard deviations for releases at the start of the transition ($t_d = 0$). At the start of the transition the boundary layer is still significantly convective. For the near-surface releases (Fig. 7a), both the LSM and the LES mean plume heights are significantly greater than the release height. The LSM mean plume height deviates by about 100 m (12% difference) from the LES at the maximum point, but overall the LSM is in good agreement with the LES. The standard deviations in Fig. 7a indicate a closer agreement for the spread of the LSM and LES plumes. For the mid-level releases there is close agreement between the LES and LSM (Fig. 7b). For the high-level releases, whilst the mean plume heights differ by about 200 m, the plume spreads are much closer (Fig. 7c).

In contrast, Fig. 8 shows the mean plume heights and standard deviations for releases at $t_d = 1200$ s. For the near-surface releases at a height of 100 m (Fig. 8a), the LSM significantly over-predicts both the mean plume height (by 400 m after 10,000 s) and the spread. For the mid-level releases (Fig. 8b), the LSM produces a mean height that remains close to the release height, in agreement with the LES; however, it over-predicts the spread. For the high-level releases (Fig. 8c), the LSM again over-predicts the spread of the plume relative to the LES. The over-dispersion of particles by the LSM at times after the switch-off of surface sensible heat flux suggests that the turbulence parameters supplied to the LSM are not fully describing the state of the boundary layer during this period. The effect of stratification is not fully represented in the LSM.

The modified LSM adjusts the vertical velocity variance to account for the partitioning between waves and turbulence in the stratified regions. Mean plume heights and spreads simulated using the modified LSM are shown in Fig. 8. For the low-level releases (Fig. 8a), the LES shows the mean plume height ascending slightly but remaining close to the height of release, indicating low levels of turbulent mixing. This behaviour is captured well by the modified LSM, with the mean plume height remaining within 50 m of the LES after 10,000 s, compared to 400 m in the case of the LSM. The spread of the modified LSM is also much closer to the LES than the LSM spread is. For the mid-level releases (Fig. 8b), all three models are in agreement for the mean height which deviates little from the middle of the boundary layer, while the spread given by the modified LSM agrees more closely with the LES than the LSM does. For the high-level releases (Fig. 8c), the modified LSM is in close agreement with the LES for both the mean height and spread.

3.3 Observed forcing

For the LES driven by the observed forcing, area-averaged boundary-layer properties at selected times are presented in Fig. 9. The area-averaged potential-temperature profile during the period of positive surface sensible heat flux (Fig. 9a) is that typical of a clear-sky CBL. As the heat flux decreases and becomes negative, a shallow SBL develops, deepening over time. In the residual layer above the developing SBL, the potential temperature has a slight positive gradient as discussed by Grant (1997) and Pino et al. (2006). As the sensible heat flux becomes negative in the lowest part of the boundary layer, the sensible heat flux in the residual layer tends to zero.

To calculate plume statistics for the observed forcing case, the trajectories of 90,000 particles were simulated using the LES, the LSM and the modified LSM. Two particle release heights of 50 m and 500 m were used, with the 50 m release lying within the strongly positive temperature gradient of the SBL shortly after it began to develop and with the 500 m release lying near the middle of the residual mixed layer. The release time was decided upon by considering the surface heat flux, the volume-averaged vertical velocity variance, and the potential-temperature profile, to ensure particles were released during the period of rapid decay of the vertical velocity variance.

Figure 10 shows the plume mean heights and standard deviations for the low and mid-level releases after the SBL has formed. For the low-level release (Fig. 10a), the LSM greatly over-

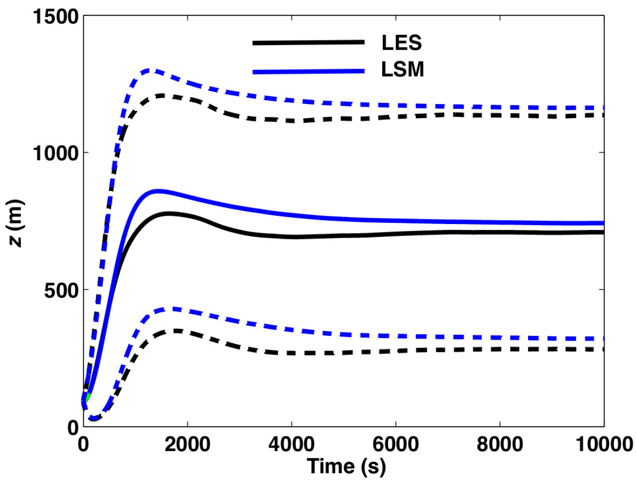

(a) Release height 100 m, at transition.

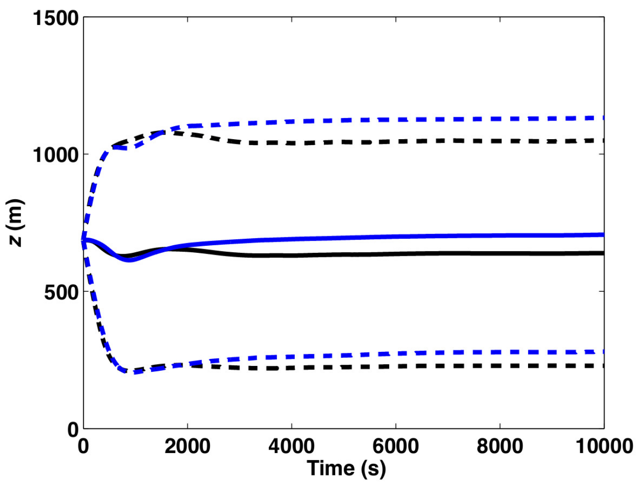

(b) Release height 687 m, at transition.

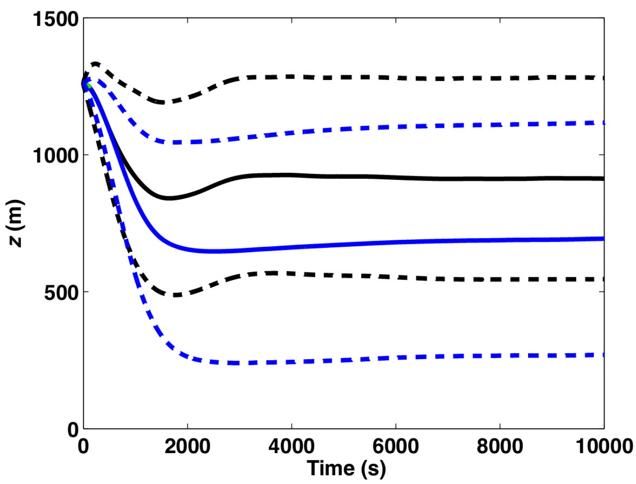

(c) Release height 1260 m, at transition.

Fig. 7: Time evolution of mean plume heights (solid lines) and ± one standard deviation (dashed) for releases at the start of the transition ($t_d = 0$) and at: (a) 100 m, (b) 687 m and (c) 1260 m for the idealized forcing. Compared are the LES (black) and LSM (blue).

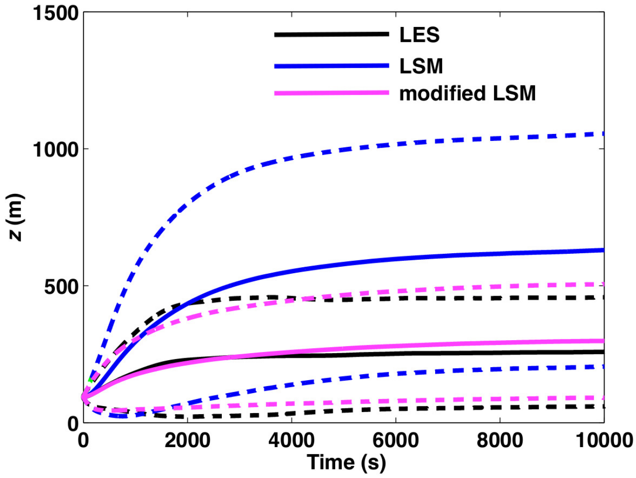

(a) Release height 100 m, after transition.

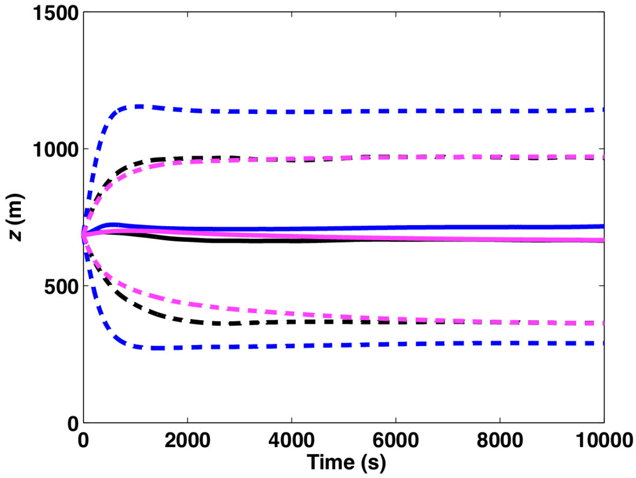

(b) Release height 687 m, after transition.

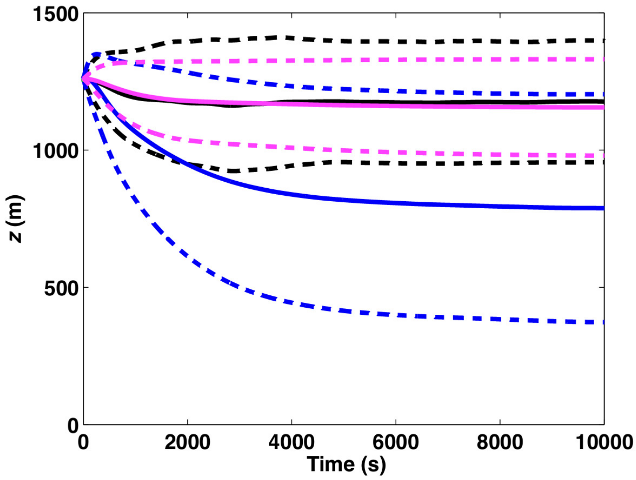

(c) Release height 1260 m, after transition.

Fig. 8: Time evolution of mean plume heights (solid lines) and $\pm$ one standard deviation (dashed) for releases after the transition (t_d = 1200 s) and at: (a) 100 m, (b) 687 m and (c) 1260 m for the idealized forcing. Compared are the LES (black), LSM (blue) and modified LSM (magenta).

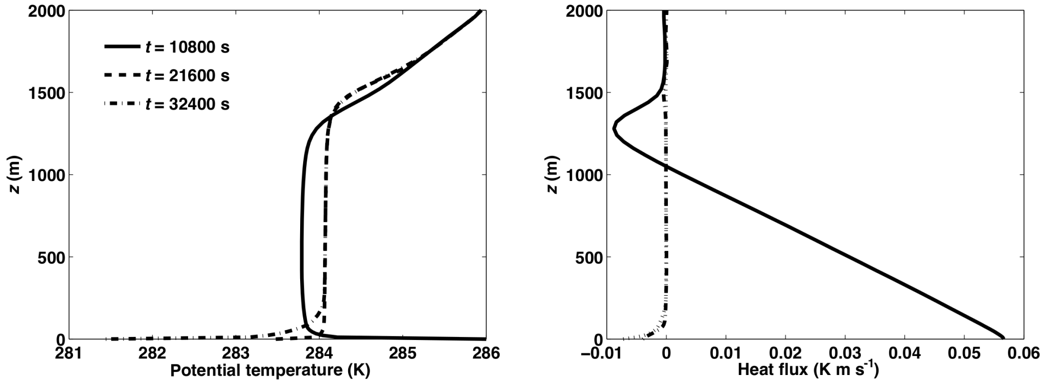

(a) (b)

Fig. 9: Vertical profiles of (a) potential temperature and (b) sensible heat flux (normalized by $\rho_0 c_p$, where ρ_0 is the surface density and c_p the specific heat capacity at constant pressure) at various times after the start of the simulation for the observed forcing. Times shown in legend.

predicts the vertical spread of the plume, which is likely to be due to the lack of representation of the stable stratification. This is a similar bias to that found for the idealized forcing. The modified LSM again predicts significantly reduced height and spread relative to the LSM, and predicts plume statistics much closer to the LES. For the mid-level release, Fig. 10b shows the LSM again over-predicting the spread of the plume, whilst the modified LSM slightly under-predicts it.

4 Conclusions

In this paper we studied the dispersion of passive tracers during the evening-transition boundary layer using both LES and LSM techniques. Whilst dispersion in steady-state boundary layers has been much simulated, only a few studies that simulate dispersion in transitional boundary layers exist. The LES, coupled to a particle model, exhibited the familiar effects of lofting of particles released near the surface in the pre-transition CBL and trapping of particles in the post-transition SBL. The LES, when forced by a sudden switch-off of the surface sensible heat flux, showed that the vertical spread of particles away from the source height was significantly reduced in the residual layer. This had the effect of increasing particle concentrations near the source height. For the LES forced by observations, the development of a SBL of depth 100 m resulted in very little vertical dispersion and even higher concentrations near the ground. These LES results thus provide more information on the problem of trapping by the post-transition SBL.

The LES results were then used to test two types of LSM. The first of these was a method to simulate dispersion in non-stationary skewed turbulence. The second, the modified LSM, also took into account the effect of stratification. The modified LSM is a simpler way of including stratification than that of Das and Durbin (2005). Both the LSM and the modified LSM were driven by flow statistics from the LES. For particle releases occurring early in the evening transition while the boundary layer is still convective, the LSM produced a fairly accurate representation of the plume statistics as simulated using the LES. For releases later in the transition, however, the LSM significantly over-predicted plume heights for near-surface releases. In con-

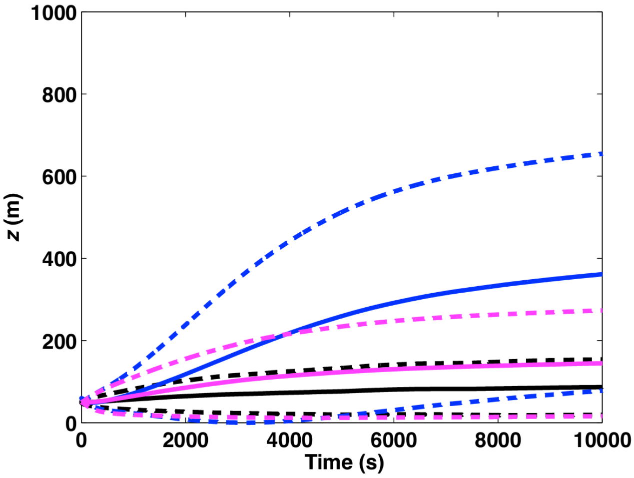

(a) Release height of 50 m, after transition ($t = 20000$ s).

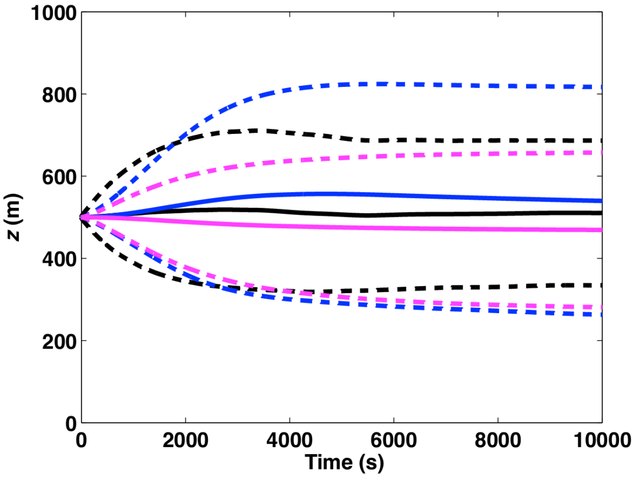

(b) Release height of 500 m, after transition ($t = 20000$ s).

Fig. 10: Mean plume heights (solid lines) and $\pm$ one standard deviation (dashed) for particle releases at $t = 20{,}000$ s from the start of the observed-forcing simulation (when a SBL is established). Compared are LES (black), LSM (blue) and modified LSM (magenta).

trast, the modified LSM corrected this bias and produced much closer agreement with the plume statistics generated by the LES.

We showed that, in modelling the stratified turbulence in residual layers and SBLs with LSMs, it is important to take account of the stratification, at least when the LSM is driven by vertical velocity variance, skewness and dissipation values from LES or measurements, which include contributions from waves and turbulence. The usual formulations of LSMs do not fully account for stratification. Our simulations also highlighted the important role of residual-layer turbulence in dispersing material above the SBL and of SBL stratification in inhibiting vertical dispersion during the evening transition. We also note that our results could apply to spatial transitions, for example for a plume moving from land to cooler water (although the analogy is not exact as space and time do not have a one-to-one relationship due to wind varying with height and to along-wind turbulence). Our results suggest that operational dispersion models would benefit from development in the treatment both of residual-layer turbulence and of stratification in evening-transition boundary layers.

Appendix - LSM including skewness and time dependence

Here we outline the formulation of the LSM used in this study. The LSM differs from the normal formulation (Eqs. 3-6) by the inclusion of skewness and time dependence. We modify $a(z, w)$ and $b(z, w)$ in Eq. 3 to now be functions of time, i.e. $a = a(z, w, t)$ and $b = b(z, w, t)$. Equations 3 and 4 have a corresponding Fokker-Planck equation, and we require this to have a solution equal to the probability density function of the positions and velocities of all air parcels ($P(w, z, t)$), i.e. we require the 'well-mixed condition' (Thomson, 1987) to be satisfied.

With the assumption that b is given by Eq. 6, manipulation of the Fokker-Planck equation will allow the determination of $a(z, w, t)$ for a given form of $P(w, z, t)$. The Fokker-Planck equation can be written in terms of the probability flux in the w direction, ϕ, as

$$\frac{\partial \phi}{\partial w} = -\frac{\partial P}{\partial t} - \frac{\partial}{\partial z}(wP), \tag{14}$$

where

$$\phi = aP - \frac{\partial}{\partial w}\left(\frac{C_0 \epsilon}{2} P\right), \tag{15}$$

and the boundary condition of no flux at infinity is

$$\phi \to 0 \text{ as } |w| \to \infty. \tag{16}$$

The procedure for deriving the LSM is to first prescribe a form for P, whether skewed, time-dependent or both, and then determine ϕ using Eqs. 14 and 16. Once ϕ is determined, $a(z, w, t)$ can be found from Eq. 15.

Including skewness

In order to include skewness, P is specified, following Baerentsen and Berkowicz (1984), as the weighted sum of two Gaussian distributions

$$P = F_1 P_1 + F_2 P_2, \tag{17}$$

where

$$P_{1,2} = \frac{1}{\sqrt{2\pi}\sigma_{1,2}} \exp\left[-\frac{1}{2}\left(\frac{w - w_{1,2}}{\sigma_{1,2}}\right)^2\right], \tag{18}$$

and F_1 and F_2 are the weights. At this stage P is assumed time independent. We then follow Luhar and Britter (1989) and substitute Eqs. 17 and 18 into Eq. 14 and integrate with respect to w. The expression for ϕ for the time independent case (ϕ_s) is then found to be

$$\phi_s = -\frac{1}{2}\left(1 + \mathrm{erf}\frac{v_1}{\sqrt{2}}\right)\frac{\partial}{\partial z}(F_1 w_1) - \frac{1}{2}\left(1 + \mathrm{erf}\frac{v_2}{\sqrt{2}}\right)\frac{\partial}{\partial z}(F_2 w_2)$$
$$+ P_1\sigma_1\left\{\left(\frac{\partial}{\partial z}(F_1\sigma_1) + \frac{F_1 w_1}{\sigma_1}\frac{\partial w_1}{\partial z}\right) + \left(F_1\frac{\partial w_1}{\partial z} + \frac{F_1 w_1}{\sigma_1}\frac{\partial \sigma_1}{\partial z}\right)v_1 + F_1\frac{\partial \sigma_1}{\partial z}v_1^2\right\}$$
$$+ P_2\sigma_2\left\{\left(\frac{\partial}{\partial z}(F_2\sigma_2) + \frac{F_2 w_2}{\sigma_2}\frac{\partial w_2}{\partial z}\right) + \left(F_2\frac{\partial w_2}{\partial z} + \frac{F_2 w_2}{\sigma_2}\frac{\partial \sigma_2}{\partial z}\right)v_2 + F_2\frac{\partial \sigma_2}{\partial z}v_2^2\right\} \quad (19)$$

where

$$v_1 = \frac{w - w_1}{\sigma_1} \quad (20)$$

and

$$v_2 = \frac{w - w_2}{\sigma_2}. \quad (21)$$

Following Hudson and Thomson (1994), the values of F_1, F_2, w_1, w_2, σ_1 and σ_2 are set by ensuring that the variance (σ_w^2) and skewness ($S = \overline{w^3}/\sigma_w^3$) of P match the values from the LES, by imposing the constraints that the integral of P is one and the mean of w is zero, and by making the choice $w_1/\sigma_1 = -w_2/\sigma_2 = S^{1/3}$. This yields

$$w_1 = \alpha\sigma_1, \quad (22)$$
$$w_2 = -\alpha\sigma_2, \quad (23)$$
$$F_1 = \sigma_2/(\sigma_1 + \sigma_2), \quad (24)$$
$$F_2 = \sigma_1/(\sigma_1 + \sigma_2), \quad (25)$$
$$\sigma_1 = \sigma_2 + \gamma/\beta, \quad (26)$$

and

$$\sigma_2 = \frac{1}{2}\{\sqrt{\gamma^2/\beta^2 + 4\beta} - \gamma/\beta\} \quad (27)$$

where $\alpha = S^{1/3}$, $\beta = \sigma_w^2/(1+\alpha^2)$ and $\gamma = \overline{w^3}/(3\alpha + \alpha^3)$. The choice $w_1/\sigma_1 = -w_2/\sigma_2 = S^{1/3}$ ensures P is Gaussian for $S = 0$.

Including time dependence

The above derivation can now be repeated, but without assuming that P is time independent. The integral of P with respect to w can be written as

$$\int_{-\infty}^{w} P(w', z, t)\, dw' = T_1 + T_2, \quad (28)$$

where T_1 and T_2 are the contributions from the Gaussian distributions P_1 and P_2 and w' is a dummy variable. Using Eq. 14, the expression for ϕ including both skewness and time-dependence is

$$\phi = -\frac{\partial}{\partial t}(T_1 + T_2) + \phi_s \quad (29)$$

where the tendencies of T_1 and T_2 are given by

$$\frac{\partial}{\partial t}T_1 = \frac{1}{2}\left(\mathrm{erf}\frac{v_1}{\sqrt{2}} + 1\right)\frac{\partial F_1}{\partial t} - P_1\sigma_1\left[\frac{F_1}{\sigma_1}\frac{\partial w_1}{\partial t} + \frac{F_1}{\sigma_1}\frac{\partial \sigma_1}{\partial t}v_1\right], \quad (30)$$
$$\frac{\partial}{\partial t}T_2 = \frac{1}{2}\left(\mathrm{erf}\frac{v_2}{\sqrt{2}} + 1\right)\frac{\partial F_2}{\partial t} - P_2\sigma_2\left[\frac{F_2}{\sigma_2}\frac{\partial w_2}{\partial t} + \frac{F_2}{\sigma_2}\frac{\partial \sigma_2}{\partial t}v_2\right]. \quad (31)$$

References

Baerentsen JH, Berkowicz R (1984) Monte Carlo simulation of plume dispersion in the convective boundary layer. Atmos Environ 18:701–712

Beare RJ, Edwards JM, Lapworth AJ (2006) Simulation of the observed evening transition and nocturnal boundary layers: large-eddy simulation. Q J R Meteorol Soc 132:81–99

Box GEP, Müller ME (1958) A note of the generation of random normal deviates. Ann Mathemat Stat 29(2):610–611

Carvalho JC, Degrazia GA, Anfossi D, Goulart AG, Cuchiara GC, Mortarini L (2010) Simulating the characteristic patterns of the dispersion during sunset PBL. Atmos Res 98:274–284

Das SK, Durbin PA (2005) A Lagrangian stochastic model for dispersion in stratified turbulence. Phys Fluids 17:025,109

van Dop H, Nieuwstadt FTM, Hunt JCR (1985) Random walk models for particle displacements in inhomogeneous unsteady turbulent flows. Phys Fluids 28:1639–1653

Goulart A, Degrazia G, Rizza U, Anfossi D (2003) A theoretical model for the study of convective turbulence decay amd comparison with large-eddy simulation data. Boundary-Layer Meteorol 107:143–155

Grant ALM (1997) An observational study of the evening transition boundary-layer. Q J R Meteorol Soc 123:657–677

Gray MEB, Petch J, Derbyshire SH, Brown AR, Lock AP, Swann HA, Brown PRA (2004) Version 2.3 of the Met Office large eddy model: Part II. Scientific Documentation, Met Office, UK, *51 pp*

Hudson B, Thomson DJ (1994) Dispersion in convective and neutral boundary-layers using a random walk model. Turbulence and Diffusion Note 210, Met Office, UK, *43 pp*

Kemp JR, Thomson DJ (1996) Dispersion in stable boundary layers using large-eddy simulation. Atmos Environ 30:2911–2923

Luhar AK, Britter RE (1989) A random walk model for dispersion in inhomogeneous turbulence in a convective boundary layer. Atmos Environ 23:1911–1924

Mason PJ (1992) Large-eddy simulation of dispersion in convective boundary layers with wind shear. Atmos Environ 26A:1561–1571

Nieuwstadt FTM, Brost RA (1986) The decay of convective turbulence. J Atmos Sci 43:532–546

Pino D, Jonker HJJ, de Arellano JVG, Dosio A (2006) Role of shear and the inversion strength during sunset turbulence over land: characteristic length scales. Boundary-Layer Meteorol 121:537–556

Rodean HC (1997) Stochastic Lagrangian Models of Turbulent Diffusion, *Amer. Meteorol. Soc.*, 84 pp

Sawford BL (1986) Generalized random forcing in random walk turbulent dispersion models. Phys Fluids 29:3582–3586

Sorbjan Z (1997) Decay of convective turbulence revisited. Boundary-Layer Meteorol 82:501–515

Stull RB (1988) An introduction to boundary layer meteorology. Springer, *670 pp*

Taylor GI (1921) Diffusion by continuous movements. Proc Lond Mathemat Soc s2-20:196–212

Thomson DJ (1984) Random walk modelling of diffusion in inhomogeneous turbulence. Q J R Meteorol Soc 110:1107–1120

Thomson DJ (1987) Criteria for the selection of stochastic models of particle trajectories in turbulent flows. J Fluid Mech 180:529–556

Weil JC (1990) A diagnosis of the asymmetry in top-down and bottom-up diffusion using a Lagrangian stochastic model. J Atmos Sci 47:501–515

Weil JC, Sullivan PP, Moeng CH (2004) The use of large-eddy simulations in Lagrangian particle dispersion models. J Atmos Sci 61:2877–2887

Willis GE, Deardorff JW (1976) A laboratory model of diffusion into the unstable planetary boundary layer. Q J R Meteorol Soc 102:427–445

Willis GE, Deardorff JW (1978) A laboratory study of dispersion from an elevated source within a modelled convective planetary boundary layer. Atmos Environ 12:1305–1311

Wilson JD, Sawford BL (1996) Review of Lagrangian stochastic models for trajectories in the turbulent atmosphere. Boundary-Layer Meteorol 78:191–210

Wilson JD, Thurtell GW, Kidd GE (1981) Numerical simulation of particle trajectories in inhomogeneous turbulence. III: Comparison of predictions with experimental data for the atmospheric surface-layer. Boundary-Layer Meteorol 21:443–463